



1    **Heterogeneous Phototransformation of Halogenated Polycyclic Aromatic**  
2    **Hydrocarbons: Influencing Factors, Mechanisms and Products**

3    Yueyao Yang<sup>1, 2, 3</sup>, Yahui Liu<sup>1, 2, 3</sup>, Guohua Zhu<sup>2</sup>, Bingcheng Lin<sup>2</sup>, Shanshan Zhang<sup>1, 2, 3</sup>, Xin Li<sup>1, 2, 3</sup>,  
4    Fangxi Xu<sup>4</sup>, He Niu<sup>4</sup>, Rong Jin<sup>2, \*</sup>, Minghui Zheng<sup>1, 2, 3</sup>

5

6    <sup>1</sup> State Key Laboratory of Environmental Chemistry and Ecotoxicology, Research Center for Eco-  
7    Environmental Sciences, Chinese Academy of Sciences, Beijing, 100085, China

8    <sup>2</sup> School of Environment, Hangzhou Institute for Advanced Study, University of Chinese Academy of  
9    Sciences, Hangzhou, 310024, China

10    <sup>3</sup> College of Resource and Environment, University of Chinese Academy of Sciences, Beijing, 100049,  
11    China

12    <sup>4</sup> Zhejiang Taizhou Ecological and Environmental Monitoring Center, Taizhou 318000, China

13    \* Correspondence to: jinrong@ucas.ac.cn (R. Jin)



## 14    **ABSTRACT**

15        Chlorinated and brominated polycyclic aromatic hydrocarbons (XPAHs) are emerging pollutants  
16        widely found in atmospheric particulate matter (PM). However, their environmental transformation  
17        mechanisms remain poorly understood. In this study, we collected PM samples of varying sizes over a  
18        year for XPAH analysis and found the average concentrations of XPAHs peaked in winter and were  
19        dominated by PM<sub>1</sub> (47.0%). Correlation analysis with relevant meteorological parameters showed strong  
20        associations between XPAH fluctuations and PM, temperatures, and humidity. Hence, controlled  
21        laboratory experiments were conducted to explore the influence of particle size, sunlight duration,  
22        temperature, humidity, and oxidant concentrations on XPAH transformation. Our results indicated that  
23        the transformation rates of XPAHs were influenced by the parent polycyclic aromatic hydrocarbon  
24        structures, with phenanthrene < fluoranthene < pyrene < benz[a]anthracene  $\approx$  anthracene <  
25        benzo[a]pyrene, as well as the substitution of halogens: chlorinated < brominated. Furthermore, the  
26        photo irradiation promoted the heterogeneous transformation of XPAHs, with this process being  
27        accelerated by the increased concentrations of reactive oxygen species and elevated temperature,  
28        peaking at the humidity level of 45%. The transformation products were identified by nontarget analysis.  
29        We then proposed phototransformation pathways for XPAHs, suggesting a mechanism involving  
30        dechlorination followed by oxidation. Predictions were made regarding the persistence, bioaccumulation,  
31        long-range transportation, and toxicities of XPAHs and their transformation products, showing a  
32        decrement in environmental risks as the transformation progressed. This study provides novel insights  
33        into the primary influencing factors for particulate XPAH variations and the mechanisms of  
34        heterogeneous phototransformation.

35  
36    **KEYWORDS:** Photochemistry; Influencing factors; Heterogeneous phototransformation;  
37    Transformation mechanism; Transformation pathways;

38



## 39 1. Introduction

40 Chlorinated and brominated polycyclic aromatic hydrocarbons (CIPAHs and BrPAHs; XPAHs) are  
41 halogenated derivatives of polycyclic aromatic hydrocarbons (PAHs) that have garnered considerable  
42 attention in recent years due to their heightened persistence, toxicity, and bioaccumulation relative to  
43 their parent PAHs (Jin et al., 2017b; Ma et al., 2013; Nishimura et al., 2017; Ohura et al., 2013). At  
44 present, research on XPAHs primarily encompasses the following aspects: (1) Establishment of pre-  
45 treatment and instrumental methods (Jin et al., 2023; Liu et al., 2019b; Noro et al., 2023; Sei et al., 2021;  
46 Takikawa et al., 2023), (2) Environmental detection across various environmental media (Jin et al., 2020;  
47 Xie et al., 2021), and (3) Identification of anthropogenic sources. XPAHs have been reported to exist in  
48 the air (Jin et al., 2017c; Kakimoto et al., 2014; Nilsson and Ostman 1993), soil (Sun et al., 2013; Zhang  
49 et al., 2006), water (Shiraishi et al., 1985), sediment (Ohura et al., 2015), and organisms (Jin et al.,  
50 2017a; Liu et al., 2019b; Nishimura et al., 2017; Ohura et al., 2015; Xia et al., 2019). The sources, such  
51 as industrial thermal processes (Yang et al., 2022b), electronic waste decomposition (Wang et al., 2022),  
52 and vehicular emissions (Deng et al., 2023) have been identified, by detection of XPAHs in the stack gas  
53 and fly ash emitted from these sources (Jin et al., 2017b; Nishimura et al., 2017; Yang et al., 2022a).  
54 However, a significant aspect of research appears to have been overlooked: the environmental  
55 transformation. Variations in the transformation mechanisms of XPAH congeners in environmental  
56 matrices can result in differences in their environmental fate and associated risks.

57 The photochemical processes have been verified to represent a marked elimination pathway for  
58 atmospheric organic chemical species (Hu et al., 2021; Laskin et al., 2015; Malecha and Nizkorodov  
59 2016). For example, PAHs have been confirmed to undergo oxidation (Zhu et al., 2022), or thorough  
60 fragmentation (Hu et al., 2021; Zhang et al., 2024) under atmospheric photochemical reactions.  
61 Therefore, despite the absence of direct study, given their structural similarities to PAHs, XPAHs also  
62 possess the potential to undergo similar processes. A study by Ohura et al. also confirmed the  
63 photochemical transformation of CIPAHs when being exposed to light in cyclohexane solvent (Ohura et  
64 al., 2008). Field observations provided additional evidence suggesting that the photochemistry plays a  
65 crucial role in atmospheric XPAH transformation. For instance, certain studies have shown that  
66 concentrations of CIPAHs in particulate matter (PM) were slightly higher during nighttime than during  
67 daytime (Ma et al., 2013; Ohura et al., 2013), indicating that daytime photochemistry contributed to the  
68 transformation of XPAHs. For BrPAHs, although no direct nighttime versus daytime concentration



69 comparison has been conducted, prior research indicated that BrPAHs might exhibit greater instability  
70 under photo irradiation than CIPAHs (Ohura et al., 2009).

71 Heterogeneous reactions were identified to be the key mechanisms driving the transformation of  
72 atmospheric organic compounds, e.g., PAHs (Jia et al., 2019), during these photochemistry processes  
73 (Zhang et al., 2023). Atmospheric PM acts as a significant carrier for both environmental pollutants and  
74 catalysts, serving as a medium for heterogeneous reactions. These reactions could be influenced by  
75 various environmental factors. For instance, the reactive oxygen species (ROS) have been identified to  
76 accelerate the phototransformation of polychlorinated naphthalene (PCNs), which are two-ring CIPAHs,  
77 on the surface of silica gel (Kang et al., 2021). In addition, the temperature and humidity have been  
78 noted to influence the lifetime of atmospheric organics (Shiraiwa et al., 2011). For example, the  
79 heterogeneous oxidation mechanisms of organophosphate flame retardants were found to be  
80 significantly affected by humidity (Liu et al., 2019a). In the case of particulate XPAHs, heterogeneous  
81 reactions may also play a crucial role in their transformation. However, the influencing factors, specific  
82 mechanisms, pathways, and products remain unclear, necessitating further exploration.

83 This study aims to unravel the mechanisms, influencing factors, pathways, and products of XPAH  
84 heterogeneous transformation on PM. To achieve this, we conducted field studies complemented by  
85 meticulously designed laboratory experiments and nontarget organic compound analysis. Initially, we  
86 collected year-range particle samples of various sizes along with relevant meteorological data. These  
87 samples were subsequently analyzed for XPAHs. Through multivariate parameter analysis, we explored  
88 XPAH fluctuations correlated with meteorological data to pinpoint key influencing factors. Subsequently,  
89 controlled laboratory experiments were designed and conducted to unveil the heterogeneous  
90 transformation of XPAHs under the influence of particle size, humidity, temperature, and atmospheric  
91 oxidant content. The persistence, bioaccumulation, long-range transportation, and toxicities of the  
92 transformation products were then assessed to determine the environmental risks associated with XPAH  
93 transformation. Therefore, the findings of this study contribute comprehensive insights into the  
94 mechanisms and environmental risks involved in the fate of XPAHs in the environment.

## 95 **2. Materials and methods**

### 96 **2.1 Experimental materials**

97 In this study, a comprehensive investigation was conducted on 41 XPAHs with 2 to 5 benzene rings,  
98 along with an analysis of the corresponding parent PAHs. The parent PAHs are abbreviated as follows:



99 Nap (naphthalene), Phe (phenanthrene), Ant (anthracene), Fluor (fluoranthene), Pyr (pyrene), BaA  
 100 (benz[a]anthracene), and BaP (benzo[a]pyrene). The congeners in the C1PAH and BrPAH groups are  
 101 described as Cl-, Cl<sub>2</sub>-, Cl<sub>3</sub>-, Cl<sub>4</sub>-, Br-, and Br<sub>2</sub>-, indicating the presence of monochlorinated, dichlorinated,  
 102 trichlorinated, tetrachlorinated, monobrominated, and dibrominated PAH derivatives, respectively, with  
 103 the numbers denoting the substituting positions. Specific names, abbreviations, and molecular structures  
 104 of 20 C1PAHs and 21 BrPAHs are listed in **Table S1**. As reported in our previous study (Jin et al., 2017c),  
 105 standards, isotopically labeled internal standards, and recovery standards for XPAHs and PAHs were  
 106 commercially obtained.

## 107 **2.2 Sample collection and extraction**

108 Atmospheric particles of three sizes (PM<sub>1</sub>, PM<sub>2.5</sub>, PM<sub>10</sub>) were collected in Hangzhou from March  
 109 2023 to February 2024 using medium-flow samplers (Wuhan Tianhong Instruments Co., Ltd., China).  
 110 These samplers were positioned atop a school building at a height of approximately 15 meters above  
 111 ground level. The sampling site (30° 8' 15" N, 120° 4' 17" E) was situated in the Xihu District of  
 112 Hangzhou, with no industrial area within a five-kilometer radius. Samples were collected in monthly  
 113 cycles, at a flow rate of 0.1 m<sup>3</sup>/min. Quartz fiber filters were employed to capture particles. Subsequently,  
 114 samples were collected, dried, weighed, and stored at -18 °C.

115 Samples were extracted with a mixture of dichloromethane and hexane (1:4, v: v) by an auto-  
 116 Soxhlet extractor (Universal Extractor E-800, Buchi, Germany). The extracted samples were then  
 117 purified using an active silica column and concentrated to 50 µL using a rotary evaporator and nitrogen  
 118 blower. Specific processes for the extraction and clean-up processes can be found in our previous study  
 119 (Jin et al., 2017c).

## 120 **2.3 Experiments design for heterogeneous transformation of particulate XPAHs**

121 In this study, we designed a photo-transformation device that provided complete confinement and  
 122 precise control over the experimental conditions. The reaction unit employed a xenon lamp (light  
 123 intensity: 100 mW·cm<sup>-2</sup>) as the primary light source with an AM1.5 filter, which can achieve a good fit  
 124 with the sunlight spectrum, effectively simulating the outdoor solar radiation (Cao et al., 2020; Wang et  
 125 al., 2020). The entire photolysis reaction unit comprises a gas supply, mass flowmeters, a dryer (with  
 126 molecular sieve and color silica gel), a bubbler containing Milli-Q water, a xenon lamp, an optical  
 127 reactor, a quartz reaction vessel, a temperature control system, gas absorption bottles, and a relative  
 128 humidity monitoring component (**Fig. 1a**). To accurately emulate atmospheric conditions, model



129 particles and a composite mixture comprising 41 XPAHs were meticulously prepared. Sequentially, 20  
130  $\mu\text{L}$  of the XPAHs mixture (1 mg/L) or individual congener solution was deposited onto the surface of the  
131 prepared layer of silica particles ( $M_{\text{XPAHs}}: M_{\text{PM}} = 2\mu\text{g/g}$ ) (**Fig. 1b** and **Fig. S1**). The settings of the  
132 concentrations were based on previous studies on the XPAH concentrations per particle mass (Jin et al.,  
133 2017a; Jin et al., 2018). Specific information on the devices and experiments are described in **Text S1**.

134 To comprehensively explore the impact of various factors, including particle sizes (100 nm, 2  $\mu\text{m}$ ,  
135 10  $\mu\text{m}$ ), temperatures (10°C, 20°C, 30°C), humidity (RH=30%, 45%, 60%), oxidant concentrations (0%  
136 (+ tert-butyl alcohol; TBA), 0%, 1%, 3%, 5%, 10%), and irradiation duration (0 min, 10 min, 30 min, 60  
137 min, 180 min), on the phototransformation mechanism of XPAHs, a series of experiments were  
138 conducted (**Text S1**). The reacted gas was directed into a toluene solution for analysis of XPAHs in the  
139 tail gas, with less than 1% of the XPAHs escaping through volatilization during the reaction time. Dark  
140 control groups were conducted in each experiment to ensure that the difference between the two sets of  
141 experiments was due to the transformation effect caused by photo irradiation. Upon completion of the  
142 reactions, the particle layer within the reaction vessel was sonicated with 200  $\mu\text{L}$  of toluene, followed by  
143 centrifugation of the supernatant. The resulting solution was then transferred into a centrifuge tube for  
144 subsequent product analysis.

#### 145 **2.4 Instrumental analysis**

146 Analysis of the XPAHs and PAHs was conducted using gas chromatography coupled with magnetic  
147 sector high-resolution mass spectrometry (HRGC-HRMS, DFS, Thermo Fisher Scientific, USA)  
148 equipped with an electron ionization source. Specific information on the parameters for the oven and MS  
149 can be found in our previous study (Jin et al., 2017a). The analytical program and instrumental  
150 parameters for the analysis of PAHs were set according to “CalEPA Method 429”.

151 Non-target analysis of the transformation products of XPAHs was performed using a Trace 1310  
152 GC coupled to a quadrupole-Orbitrap MS (Thermo Fisher Scientific, USA). Data were collected and  
153 processed using Thermo Scientific TraceFinder 5.1 software. High-resolution mass spectra of unknown  
154 compounds were deconvoluted into pure spectra using the Deconvolution Plugin of TraceFinder  
155 software and then verified against the standard mass spectra from the commercial library NIST 2014.  
156 Specific information on the non-target analysis was shown in **Text S2**.

#### 157 **2.5 Environmental behavior and toxicity assessment of XPAHs and their transformation products**

158 To assess the ecological risk and environmental characteristics—specifically, persistence, long-



range transport potential, and bioaccumulation—of transformation products of XPAHs, this study employed the KOWWIN, KOAWIN, BCFBAF, and Level III fugacity models within EPI Suite 4.1 to compute various physicochemical properties of compounds. Essential environmental parameters, including molecular weight, octanol-water partition coefficient ( $K_{ow}$ ), air-water partition coefficient ( $K_{aw}$ ), and half-lives in air, water, and soil, were subsequently introduced into the Pov-LRTP tool (Concha and Manzano 2023). Subsequently, the P-B-LRTP score is developed based on persistence (Pov), characteristic travel distance (CTD), and transfer efficiency (TE) values to prioritize the screened compounds. The respiratory toxicity model in ProTox 3.0 (Banerjee et al., 2024) was used to predict the toxicity of the products, assessing their median lethal dose (LD50) and toxicity class.

$$P - B - LRTP \text{ Score}_i = \text{LogPov} + \text{LogBAF} + \text{LogTE}$$

## 2.6 Quality assurance and quality control

For the analysis of actual atmospheric PM samples, the recovery rates of internal standards ranged from 52% to 105%. In laboratory simulation experiments, the recovery rates of XPAHs ranged from 78% to 115%, while those of PAHs ranged from 53% to 120%. These recovery rates met the requirements for the detection and analysis of persistent organic pollutants. The detection limits (LODs) ranged from 0.17 to 1.9  $\text{fg}/\text{m}^3$  for CIPAHs, and from 0.23 to 1.6  $\text{fg}/\text{m}^3$  for BrPAHs. A blank sample was analyzed together with each batch of samples, and the relative concentrations of all XPAH congeners were below the detection limits.

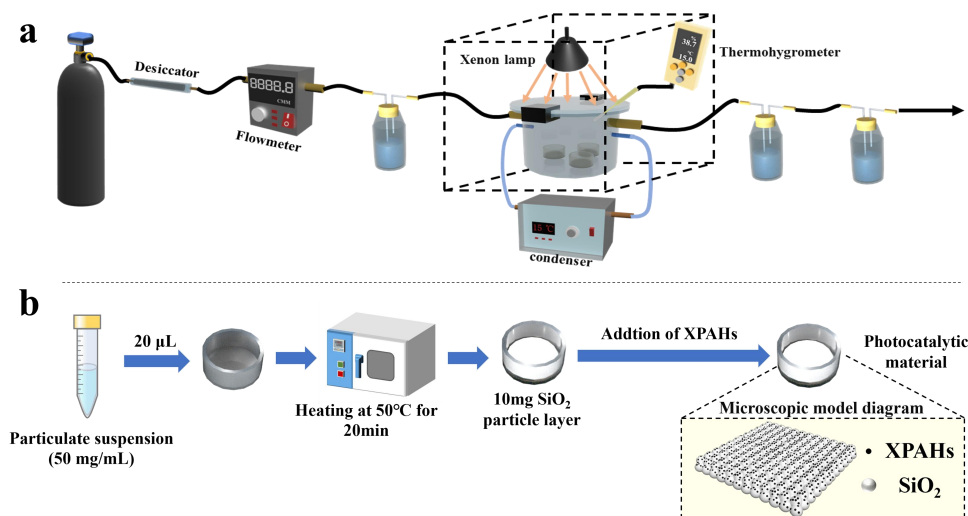


**Fig. 1.** (a) The laboratory photochemical transformation setup. (b) Particulate matter preparation process.



### 179 3. Results and discussion

#### 180 3.1 Occurrence levels and congener profiles of particulate XPAHs

181 During the sampling period, PM concentrations ranged from 41.5 to 652.7  $\mu\text{g}/\text{m}^3$ , with an average  
 182 concentration of  $130.0 \pm 167.6 \mu\text{g}/\text{m}^3$  (**Fig. S2a**).  $\text{PM}_{10}$  had the highest proportion, with an average of  
 183  $47.0\% \pm 13.5\%$ , while the proportions of  $\text{PM}_{1-2.5}$  and  $\text{PM}_{2.5-10}$  were comparable. Notably, the peak  
 184 concentration was recorded in April 2023. This surge coincided with a dust storm originating from the  
 185 north, leading to heightened levels of suspended dust in the atmosphere and a significant spike in PM  
 186 levels. Barring exceptional weather conditions, PM concentrations in other seasons were approximately  
 187 twice as high as those observed in summer and autumn.

188 The concentrations of  $\sum_{21}\text{CIPAHs}$  in the particles ranged from 0.6 to 61.5  $\text{pg}/\text{m}^3$  (mean:  $12.1 \pm$   
 189  $16.9 \text{ pg}/\text{m}^3$ ), while those of  $\sum_{18}\text{BrPAHs}$  ranged from N.D. to 5.4  $\text{pg}/\text{m}^3$  (mean:  $0.6 \pm 1.5 \text{ pg}/\text{m}^3$ ) during  
 190 the sampling period (**Fig. 2a**). These values are lower than those reported in previous studies, such as  
 191 Beijing, China ( $\sum_{19}\text{CIPAHs}$ :  $128.8 \pm 102.6 \text{ pg}/\text{m}^3$ ,  $\sum_{19}\text{BrPAHs}$ :  $9.5 \pm 13.8 \text{ pg}/\text{m}^3$ ) (Jin et al., 2017a);  
 192 Ulsan, South Korea ( $\sum_{11}\text{BrPAHs}$ :  $1.62 \text{ pg}/\text{m}^3$ ) (Vuong et al., 2020); and Shizuoka, Japan ( $\sum_{20}\text{CIPAHs}$ :  
 193  $133 \pm 53 \text{ pg}/\text{m}^3$ ) (Ohura et al., 2013). For distribution in particles of different sizes, CIPAHs had the  
 194 highest fraction in  $\text{PM}_{10}$  (mean: 45.4%, range: 29.4–65.9%) and comparable proportions in  $\text{PM}_{1-2.5}$  (mean:  
 195 28.1%, range: 13.0–52.0%) and  $\text{PM}_{2.5-10}$  (mean: 26.5%, range: 8.46–3.5%). Conversely, BrPAHs showed  
 196 no significant variance across the three particle size ranges, with concentrations of  $\text{PM}_{10}$  (mean: 35.9%,  
 197 range: 12.5–68.2%),  $\text{PM}_{1-2.5}$  (mean: 35.7%, range: 14.3–55.2%) and  $\text{PM}_{2.5-10}$  (mean: 28.4%, range: 1.25–  
 198 59.2%) (**Fig. 2b**). In total, over 70% of XPAHs were bound to particles with diameters smaller than 2.5  
 199  $\mu\text{m}$ .

200 Concentration trends of XPAH homologue groups were as follows: ClFluor > ClBaP > ClAnt >  
 201 ClPyr > ClPhe > ClBaA (**Table S2**); BrPyr > BrPhe > BrAnt > BrTriph > BrBaA > BrFluor (N.D.)  
 202 (**Table S3**). The distribution profiles of XPAH congeners in  $\text{PM}_{10}$  in Hangzhou are shown in **Fig. S2b**,  
 203 **Fig. S2c**, and **Table S4**. Among CIPAHs, 2-ClPhe/9-ClPhe, 1,5-Cl<sub>2</sub>Ant/9,10-Cl<sub>2</sub>Ant, 1-ClPyr, 3-ClFluor,  
 204 3,8-Cl<sub>2</sub>Fluor, and 6-ClBaP were found to be predominant throughout the year. This distributions aligned  
 205 with findings of prior studies (Jin et al., 2017a; KITAZAWA et al., 2006; Ma et al., 2013). It is worth  
 206 noting that 6-ClBaP, characterized by the highest molecular weight and highest toxic equivalent factor  
 207 investigated within CIPAHs investigated in our study, demonstrated the highest concentration proportion.  
 208 BrPAHs are predominantly constituted by 2-BrPhe, 9-BrPhe, 7-BrBaA, and 1,6-Br<sub>2</sub>Byr. This presented a





notable departure from previous literature which predominantly identified 3-BrFluor, 1,8-Br<sub>2</sub>Ant, and 1-BrPyr as the primary congeners of BrPAHs in atmospheric PM in Beijing (Jin et al., 2017a). This disparity underscores variances in their respective sources or transformations.

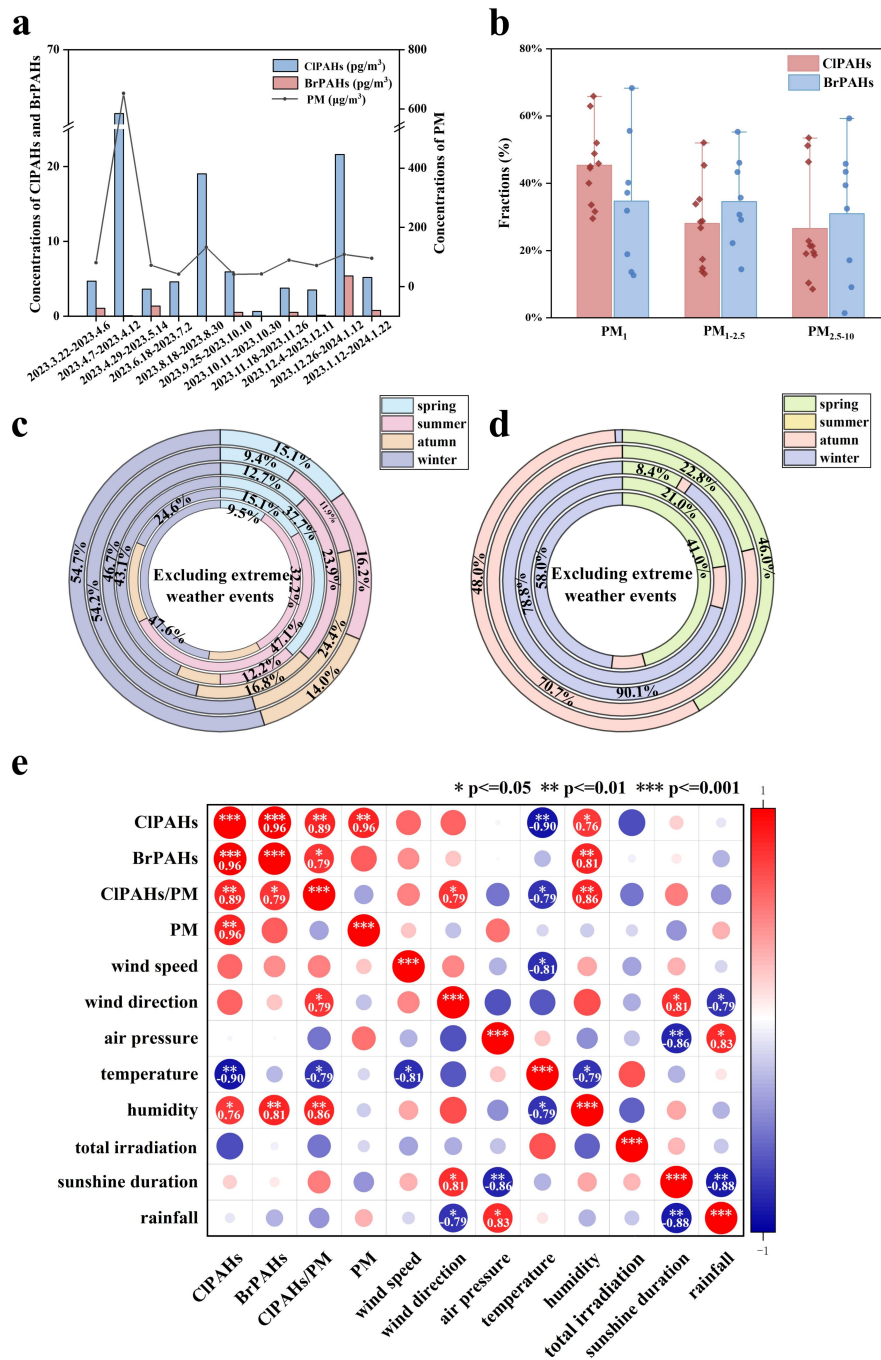
### 3.2 Key environmental factors influencing temporal variations of particulate XPAHs

Extreme weather events such as sandstorms and prolonged light rainfall have been excluded in the following discussion. The average concentrations of PM and BrPAHs reached nadirs during summer and autumn while showing higher levels in spring and winter (**Fig. S2d**). Conversely, CIPAH concentrations remained relatively stable during spring and summer, decreased in autumn, and peaked in winter. The seasonal characteristics of CIPAHs with different parent PAH structures also varied (**Fig. 2c**). Except for ClBaA, the remaining CIPAHs reached their highest concentrations during winter. ClFluor showed elevated concentrations in both spring and winter, whereas ClAnt demonstrated higher concentrations in autumn and winter. ClPhe maintained relatively consistent concentrations across the remaining three seasons. The seasonal characteristics of CIPAHs and BrPAHs (**Fig. 2d**) also differed. Concentrations of BrPAHs varied significantly with the seasons, with no congener detected in summer and high concentrations of BrPhe, BrAnt, and BrPyr in spring and winter, likely influenced by climatic conditions such as temperature and sunshine. This disparity can be attributed to the ease of generation from sources and greater atmospheric stability of CIPAHs, while BrPAHs may be subject to influences from atmospheric processes (Ohura et al., 2009).

Eight meteorological parameters were collected throughout the sampling period: wind speed, wind direction, air pressure, temperature, humidity, total irradiation, sunshine duration, and rainfall. Details are listed in **Table S5**, and the results of multifactor correlation analysis are shown in **Fig. 2e**. Pearson correlation analysis revealed significant positive correlations between CIPAHs and BrPAHs ( $P < 0.001$ ,  $R = 0.96$ ), PM ( $P < 0.01$ ,  $R = 0.96$ ), and humidity ( $P < 0.05$ ,  $R = 0.76$ ). BrPAHs exhibited a significant positive correlation with humidity ( $P < 0.01$ ,  $R = 0.81$ ). The impact of humidity was notably significant, as an increase in humidity tended to facilitate the upward adsorption of XPAHs onto PM. However, a previous study (Vuong et al., 2020) from Ulsan, South Korea has reported a negative correlation between humidity and XPAHs. This observation suggested that the relationship between XPAHs and humidity varied across different regions. Additionally, CIPAHs shew a significant negative correlation with temperature ( $P < 0.01$ ,  $R = -0.90$ ), suggesting that higher temperatures corresponded to lower CIPAH concentrations. This further elucidated the phenomenon of lower CIPAH levels observed during



239 the summer and autumn seasons. Other meteorological factors didn't show significant correlations with  
240 CIPAHs or BrPAHs ( $P > 0.05$ ), possibly due to the intricate interplay of multiple factors under natural  
241 conditions. Hence, the specific roles of meteorological conditions such as sunlight intensity, duration of  
242 sunshine, temperature, and humidity warranted further investigation.



243

244 **Fig. 2.** (a) The fluctuations of concentrations of PM,  $\Sigma_{21}$ CIPAHs, and  $\Sigma_{19}$ BrPAHs in the atmosphere. (b) The

245 proportions of CIPAHs and BrPAHs across different PM diameters. (c-d) Seasonal distributions of CIPAH (c) and



BrPAH (d) congeners, excluding events of extreme conditions, arranged from outermost to innermost layers: ClPhe, ClAnt, ClPyr, ClFluor, ClBaA, and ClBaP; BrPhe, BrAnt, BrPyr, BrTriph, and BrBaA. (e) Pearson correlation analysis between ClPAHs, BrPAHs and ClPAHs/PM with meteorological parameters (wind speed, wind direction, air pressure, temperature, humidity, total radiation, sunshine duration, and rainfall) under non-extreme weather conditions.

### 3.3 General transformation mechanisms of particulate XPAHs under photo irradiation

According to both preliminary research (Li et al., 2023) and the experimental results mentioned above, it is evident that meteorological conditions can significantly impact the concentrations and distributions of XPAHs on PM. Controlled laboratory experiments were conducted in this study to unveil the heterogeneous transformation mechanisms of XPAHs.

The transformation ratios of XPAHs were calculated based on the ratios of transformed XPAHs to the initial concentration  $((C_0 - C_t)/C_0)$ . With the increase of irradiation time, a general trend of transformation was observed across XPAH congeners (Fig. 3). Overall, the transformation rates of ClPAHs appeared to follow the sequence: ClPhe < ClFluor < ClPyr < ClBaA  $\approx$  ClAnt < ClBaP (Fig. S3). This pattern aligned with the previously reported trends in PAH photolysis rates (Phe < BaA < Ant  $\approx$  BaP) (Zhao et al., 2017), indicating strong influence by the parent PAH structures. In a combined consideration of ClPAHs and their parent PAHs, shown as “ClPAHs+PAHs” in Fig. S3, we also observed the formation of PAHs and decreases of total concentrations of ClPAHs and PAHs. This indicated that there were dechlorination of ClPAHs and simultaneous fragmentation of parent PAH structures during the transformation of ClPAHs.

In addition, the substitution numbers in the structures had a strong influence on the transformation of ClPAHs: with increment of the substitution numbers, the transformation ratios progressively decreased (Fig. 3). For example, after 1 h of irradiation, transformation ratios were approximately 20% for 3-ClPhe and 2-ClPhe/9-ClPhe, while 10% for 9,10-Cl<sub>2</sub>Phe. An exception was observed for ClAnt congeners (1,4-Cl<sub>2</sub>Ant or 1,5-Cl<sub>2</sub>Ant/9,10-Cl<sub>2</sub>Ant < 1-ClAnt/2-ClAnt or 9-ClAnt < 1,5,9,10-Cl<sub>4</sub>Ant. This difference could be attributed to the fact that the investigated low-chlorinated ClAnts are dechlorination products of high-chlorinated ClAnts. While the substitution position had some impact, it was not as significant as the number of chlorines. For instance, both 2,5-Cl<sub>2</sub>Fluor and 3,8-Cl<sub>2</sub>Fluor demonstrate comparable photolysis extents, with approximately 20% transformation after 30 min of irradiation, and transformation ratios of 68.8% and 49.4% after 3 h of irradiation, respectively.



For BrPAHs (**Fig. S4**), the overall transformation ratio ranked as follows: BrPhe < BrAnt < BrPyr  
 ≈ BrFluor < BrBaA < BrBaP. The transformation ratio ranking between BrPAHs and ClPAHs exhibited  
 disparities, implying that distinct halogen substitutions might yield diverse transformation effects.  
 BrPAHs degraded more rapidly than ClPAHs. For example, BrPyr degraded by 60% after 30 min of  
 irradiation, while ClPyr only degraded by less than 40%. Additionally, the increase in bromination  
 degree didn't appear to have a notable effect on the transformation rate of BrPAHs, which differed from  
 ClPAHs.

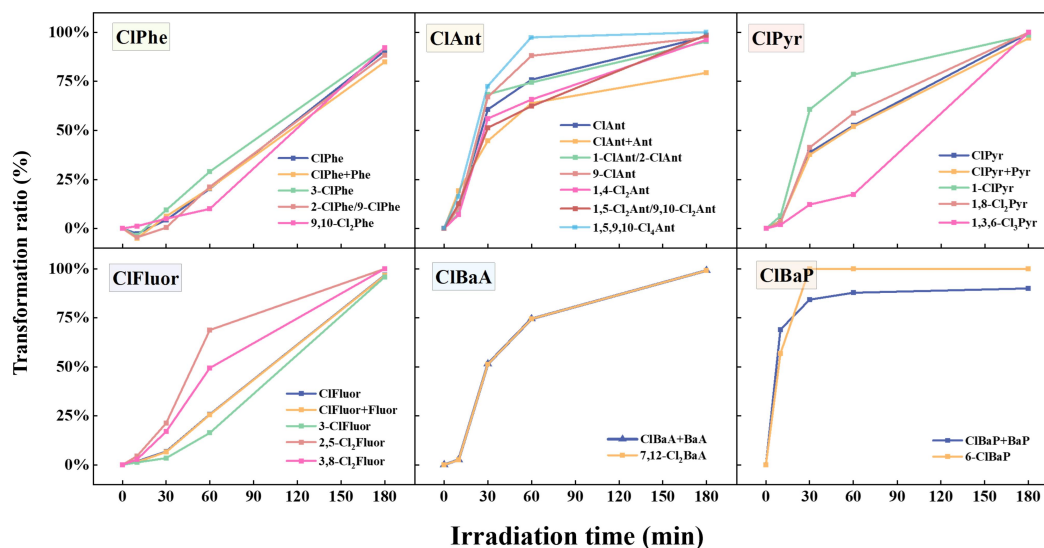


**Fig. 3.** The relationships between transformation ratios of ClPAHs and photo irradiation time.

### 3.4 Influencing factors for heterogeneous transformation of particulate XPAHs

The influencing factors, i.e., particle size, relative humidity, reactive oxygen species content, and temperature on XPAH transformation have been investigated (**Text S1**). Although previous studies have revealed variations in XPAH concentrations on particles of different sizes (Jin et al., 2017a; Lara et al., 2022; Ma et al., 2013), the influence of particle size (100 nm, 2 μm, and 10 μm) on transformation efficiency was found to be not notably significant in simulated experiments (**Fig. S5 and Text S3**).

The influence of humidity varied among ClPAHs with different parent structures (**Fig. 4a**). For instance, the transformation of ClPhe and ClFluor slowed down with increasing humidity, whereas the transformation of ClAnt, ClPyr, ClBaA, and ClBaP increased with higher humidity levels, with the highest transformation ratio observed at 45% humidity. Additionally, we found that the impact of



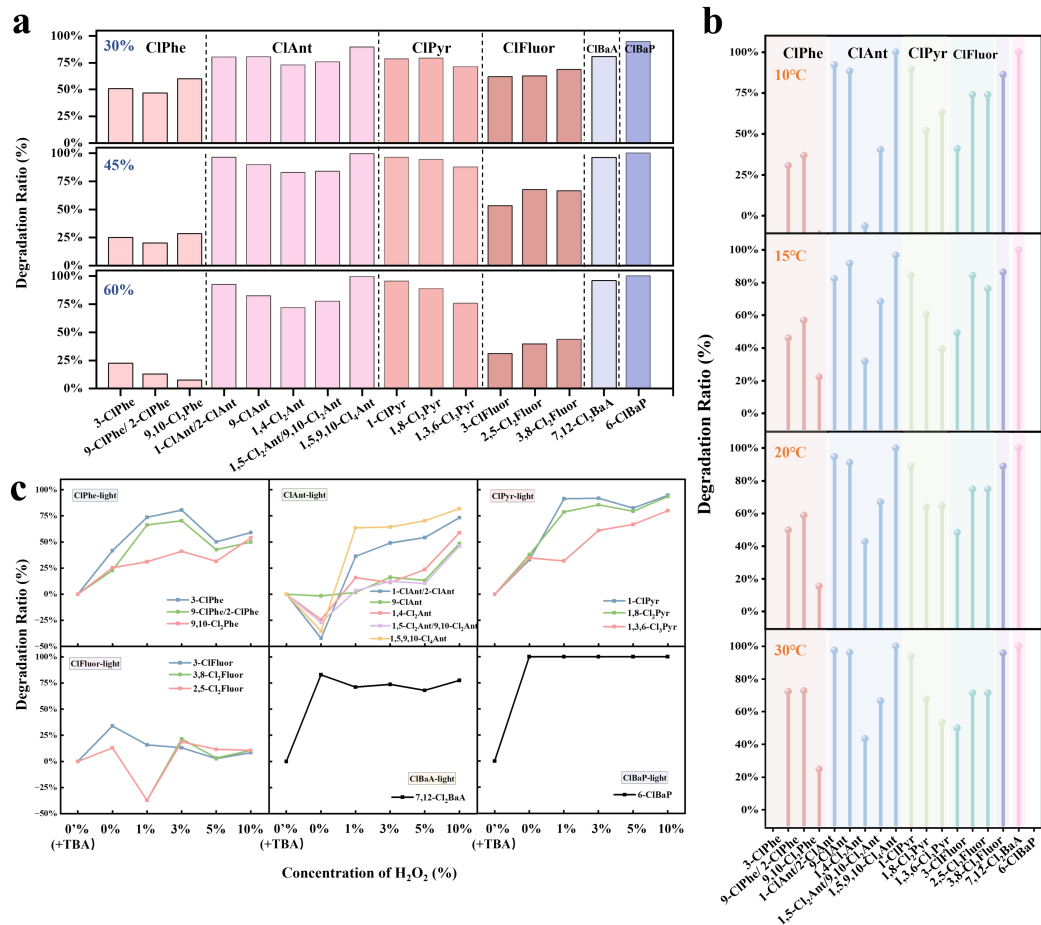
296 humidity on transformation was not consistent for ClPAH congeners in the same homologue groups. For  
297 example, transformation of 9,10-Cl<sub>2</sub>Phe decreased more sharply than the other ClPhe congeners with the  
298 increment of humidity. The combined influence of photo irradiation and humidity enhanced the  
299 transformation of individual ClPAHs (**Fig. S6**). For example, under 45% humidity, ClPyr exhibited an  
300 average transformation of 50% in darkness, while this rate increased to 75% under photo irradiation.  
301 Possible reasons could be that the addition of photo irradiation drove the formation of OH radicals ( $\cdot$ OH),  
302 which could join the breakdown of molecules (Zhang et al., 2023). In contrast, the acceleration of  
303 transformation with increasing humidity was relatively universal for BrPAHs, with the most significant  
304 effects observed within the 30-45% humidity range (**Fig. S6c** and **Fig. S6d**).

305 Transformation ratios of XPAHs increased as temperatures rose, with the most significant  
306 transformation observed at 30°C (**Fig. 4b**), indicating that the elevated temperature promote the  
307 transformation of XPAHs. The transformation ratio of each congener gradually increased with  
308 temperature compared to dark conditions (**Fig. S7a**). Under photo irradiation at the same temperature,  
309 the transformation ratios of nearly all XPAH congeners increased by more than 50% compared to dark  
310 conditions. This indicated that the breakdown of XPAH molecules was enhanced by the photo irradiation.  
311 In both photo irradiation and dark conditions, the transformation ratios of BrPAHs (**Fig. S7c** and **Fig.**  
312 **S7d**) exceeded those of ClPAHs. This phenomenon can be attributed to the lower bond energy of C-Br  
313 (291 kJ/mol) compared to C-Cl (345 kJ/mol), which is consistent with the findings of previous studies  
314 by Ohura et al (Ohura et al., 2009).

315 Adding H<sub>2</sub>O<sub>2</sub> to the reaction system simulates the effects of oxidants present in the atmosphere on  
316 the impact of XPAH transformation under photochemical conditions. The transformation of ClPAHs  
317 accelerated with the increase of H<sub>2</sub>O<sub>2</sub> concentration (**Fig. 4c** and **Fig. S8**). TBA was introduced to  
318 eliminate the  $\cdot$ OH effect in the control group. Under 1-hour photo irradiation conditions, the  
319 transformation rate ranking of ClPAHs is as follows: ClBaP > ClBaA > ClPyr > ClPhe > ClAnt >  
320 ClFluor. The transformation of ClFluor showed no significant change with H<sub>2</sub>O<sub>2</sub> content, indicating  
321 relative stability. Additionally, compared to monochlorinated compounds, the overall transformation  
322 ratios of polychlorinated compounds are relatively slower and less influenced by H<sub>2</sub>O<sub>2</sub> (except for  
323 1,5,9,10-Cl<sub>4</sub>Ant). This also suggested that the dechlorination process was more pronounced in high-  
324 chlorinated compounds, while the transformation of low-chlorinated substances was mainly due to ring-  
325 opening reactions. The situation was similar for BrPAHs, with transformation rates faster than those of



326 CIPAHs.  
327



328  
329 **Fig. 4.** Transformation ratios of CIPAHs under varying (a) humidity levels, (b) temperature conditions and (c)  
330 H<sub>2</sub>O<sub>2</sub> concentrations, with photo irradiation.

### 331 3.5 Heterogeneous transformation pathways of XPAHs under photo irradiation

332 According to the results above, there are dechlorination, direct ring-opening, or ring-opening  
333 induced by oxidation processes involved in the breakdown of XPAHs. To elucidate the specific  
334 transformation pathways of XPAHs, we conducted photolysis experiments on highly chlorinated XPAHs,  
335 including 1,4-Cl<sub>2</sub>Ant, 9,10-Cl<sub>2</sub>Phe, 1,8-Cl<sub>2</sub>Pyr, 2,5-Cl<sub>2</sub>Fluor, 7,12-Cl<sub>2</sub>BaA, and 6-ClBaP, individually.  
336 Non-target analysis was then employed to recognize the transformation products of these congeners.  
337 Specific mass spectrums can be found in **Fig. S9**, and the relative compounds are listed in **Table S6**. The



338 predominant products were quinones, ketones, hydroxyl-bearing compounds, and ring-opened products,  
339 consistent with previous findings on PAH phototransformation products (Jia et al., 2019; Zhao et al.,  
340 2017). Surprisingly, no chlorinated oxides were detected. Further analysis of the products from  
341 experiments on both ClPAHs and BrPAHs revealed no significant differences. As a result, we confirmed  
342 a hypothesis proposed in previous studies (Ohura et al., 2009) that the transformation of XPAHs  
343 underwent dehalogenation to form PAHs before oxidation.

344 The transformation pathways are presented in **Fig. 5**. According to the non-target analysis results of  
345 the photolysis products, the primary products for most ClPAHs, with the exception of ClFluor, were the  
346 parent PAHs in the initial step. And for ClFluor, the initial step involved not only the dechlorination, but  
347 also ring-opening, resulting in the generation of 2,7-dichlorofluorene and 9-chlorofluorene. Research  
348 findings suggested that in the atmosphere, the primary reactions for the destruction of aromatic  
349 compounds were the addition or substitution with  $\cdot\text{OH}$  (Dang et al., 2014). At the same time, the  
350 substitution of H or Cl in the main structures of ClPAHs or PAHs by the  $\cdot\text{OH}$  could influence the  
351 products of the next steps. Therefore, the subsequent steps might include ring opening, oxidation, or  
352 hydrolysis.

353 Specifically, there were three potential pathways for the transformation of 1,4-Cl<sub>2</sub>Ant (**Fig. 5a** and  
354 **Fig. S9a**). In the first pathway, 1,4-Cl<sub>2</sub>Ant could undergo substitution by  $\cdot\text{OH}$  to form A2 (1,4-  
355 dihydroxyanthracene, C<sub>14</sub>H<sub>10</sub>O<sub>2</sub>), which further oxidized to produce A3 (1,4-anthraquinone, C<sub>14</sub>H<sub>8</sub>O<sub>2</sub>).  
356 For the second and third pathways, 1,4-Cl<sub>2</sub>Ant underwent dechlorination to yield A1 (Ant, C<sub>14</sub>H<sub>10</sub>). The  
357 subsequent steps were then similar to those of Ant, with oxidation leading to the formation of A4 (9,10-  
358 Anthracenediol, C<sub>14</sub>H<sub>10</sub>O<sub>2</sub>), and further oxidation to A5 (9,10-Anthraquinone, C<sub>14</sub>H<sub>8</sub>O<sub>2</sub>) as the second  
359 pathway. In the third pathway, ring-opening occurred to form A6 (2-Methylnaphthalene, C<sub>11</sub>H<sub>10</sub>),  
360 followed by subsequent chain-breaking ring-opening to form A7 (Nap, C<sub>10</sub>H<sub>8</sub>), A8 (1,2,3,4-  
361 Tetrahydronaphthalene, C<sub>10</sub>H<sub>12</sub>), and A9 (2-Methoxyphenol, C<sub>7</sub>H<sub>8</sub>O<sub>2</sub>), ultimately yielding A10 (3-  
362 Nonanol, C<sub>9</sub>H<sub>20</sub>O) and A11 (3-Nonanone, C<sub>9</sub>H<sub>18</sub>O). Similar transformation pathways were observed for  
363 9,10-Cl<sub>2</sub>Phe (**Fig. 5b** and **Fig. S9b**), 1,8-Cl<sub>2</sub>Pyr (**Fig. 5c** and **Fig. S9c**), and 7,12-Cl<sub>2</sub>BaA (**Fig. 5e** and **Fig.**  
364 **S9e**), involving dechlorination to generate PAHs, followed by attack by  $\cdot\text{OH}$  to produce phenols, further  
365 oxidizing to form quinones, acids, and esters. Additionally, 9,10-Cl<sub>2</sub>Phe exhibited an additional  
366 oxidation pathway involving ring-opening oxidation, yielding B9 (9-Fluorenone, C<sub>13</sub>H<sub>8</sub>O), followed by a  
367 series of chain-breaking ring-opening reactions to sequentially generate B10 (Benzophenone, C<sub>13</sub>H<sub>10</sub>O),





368 B11 (3'-Methylacetophenone,  $C_9H_{10}O$ ), and B12 (3-Nonanone,  $C_9H_{18}O$ ). 1,8-Cl<sub>2</sub>Pyr also had two  
369 additional potential transformation pathways. In the first pathway, uniform cleavage occurred both above  
370 and below the pyrene molecule, generating C4 (Nap,  $C_{10}H_8$ ) and C5 (2-Methylnaphthalene,  $C_{11}H_{10}$ ). In  
371 the second pathway, diagonal cleavage resulted in the identification of two products: C6 (2-(2,5-  
372 dimethylphenyl)-1,4-dimethylbenzene,  $C_{14}H_{14}$ ) and C7 (4,4'-Dimethyldiphenyl,  $C_{14}H_{14}$ ). C6 underwent  
373 attack by  $\cdot OH/O_2^-$  radicals to ultimately form C8 (Benzophenone,  $C_{13}H_{10}O$ ), followed by further ring-  
374 opening cleavage to produce C9 (3'-Methylacetophenone,  $C_9H_{10}O$ ). Similarly, C10 (2-  
375 Phenylpropionaldehyde,  $C_9H_{10}O$ ) was formed by oxidation-induced chain-breaking of C8.

376 For ClFluor (**Fig. 5d** and **Fig. S9d**), the initial step involved ring-opening, generating D1 (2,7-  
377 Cl<sub>2</sub>Fle,  $C_{13}H_8Cl_2$ ) and D2 (9-ClFle,  $C_{13}H_9Cl$ ). Subsequent dechlorination and ring-opening led to the  
378 formation of D3 (4,4'-Dimethyldiphenyl,  $C_{14}H_{14}$ ), D4 (2-(2,5-dimethylphenyl)-1,4-dimethylbenzene,  
379  $C_{14}H_{14}$ ), and D5 (Benzophenone,  $C_{13}H_{10}O$ ) in the samples. In the second pathway, the initial  
380 dechlorination process resulted in the formation of D6 (Fluor,  $C_{16}H_{10}$ ), which yielded D7 (1H-Indene,  
381 2,3-dihydro-4,7-dimethyl-,  $C_{11}H_{14}$ ) and D9 (Nap,  $C_{10}H_8$ ). D7 underwent bond cleavage to form D8 (1H-  
382 Indene, octahydro-,  $C_9H_{16}$ ), while D10 (1,2-Diethylbenzene,  $C_{10}H_{14}$ ) was the ring-opening product of D9.  
383 Further oxidation (alcohol to aldehyde) sequentially yielded D11 (1,2-Dicarboxybenzene,  $C_8H_6O_4$ ) and  
384 D12 (Dibutyl phthalate,  $C_{16}H_{22}O_4$ ).

385 6-ClBaP, as a mono-chlorinated compound (**Fig. 5f** and **Fig. S9f**), exhibited the highest  
386 phototransformation ratio among all ClPAH congeners. After dechlorination, the initial step generated  
387 F1 (BaP,  $C_{20}H_{12}$ ). Among them, positions 3, 6, and 12 of BaP were particularly reactive, and  $\cdot OH$  attacks  
388 led to the formation of F2, F3, and F4 (6-Benzo[a]pyrenol, 6,12-Dihydroxybenzo[a]pyrene, and 9,12-  
389 Dihydroxybenzo[a]pyrene,  $C_{20}H_{12}O$ ), subsequently further generated F5, F6 and F7 (6-Benz[a]pyrenone,  
390 Benzo[a]pyrene-6,12-dione, and Benzo[a]pyrene-3,6-dione,  $C_{20}H_{10}O_2$ ). Under light exposure, F6  
391 underwent further oxidation and ring-opening to produce F8 (Lapachol,  $C_{15}H_{14}O_3$ ), F9 (2,6-  
392 Diisopropyl naphthalene,  $C_{16}H_{20}$ ), and F11 (Dimethyl phthalate,  $C_{16}H_{22}O_4$ ), as reported by S. Zhao et al  
393 (Zhang et al., 2023). The exploration of XPAH transformation is limited by the absence of quantification  
394 of the products. Further studies are necessary to elucidate the specific molecular assignments.

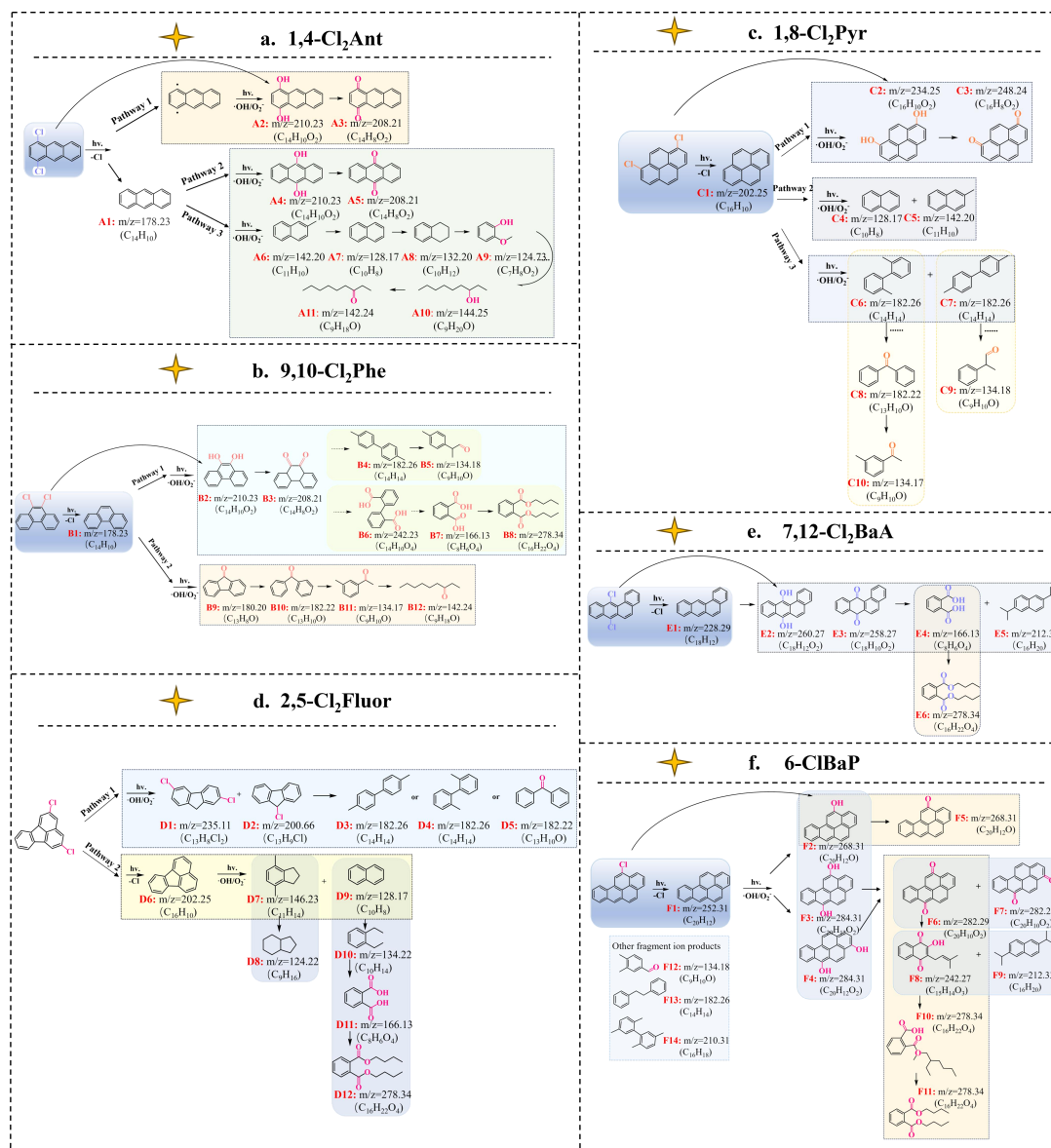


**Fig. 5.** (a-f) The transformation pathways and relative products of CIPAHs. ((a) 1,4-Cl<sub>2</sub>Ant; (b) 9,10-Cl<sub>2</sub>Phe; (c) 1,8-Cl<sub>2</sub>Pyr; (d) 2,5-Cl<sub>2</sub>Fluor; (e) 7,12-Cl<sub>2</sub>BaA; (f) 6-ClBaP).

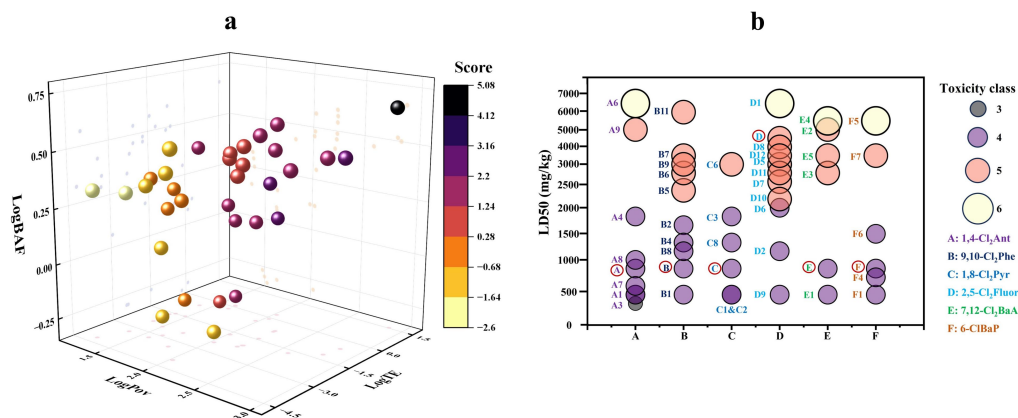
### 3.6 Assessments of persistence, bioaccumulation, long-range transportation and toxicities of XPAHs and their transformation products

Studies have suggested that transformation products of organic pollutants might exhibit distinct environmental behaviors and heightened ecological toxicity (Zhang et al., 2023). For the assessed P-B-LRTP scores of XPAHs and their transformation products in this study (Fig. 6a and Table S6), it could



be observed that as the transformation pathways progressed, the scores of the transformation products decreased. For instance, the score of 9,10-Cl<sub>2</sub>Phe was 5.07, which decreased to 2.13 after dechlorination, and further oxidation products have even lower scores ranging from 1.65 to -1.27 (9,10-Difluorenone to 1,2-Benzenedicarboxylic acid). However, there were also transformation products with relatively high scores, such as B9 (9H-Fluorene-9-one, score: 1.57) and B10 (Benzophenone, score: 1.81), which warrant special attention in future studies.

To further investigate the toxicities of these transformation products, the lethal doses (LD<sub>50</sub>) and toxicity levels (**Fig. 6b** and **Table S7**) were predicted by the respiratory toxicity model in ProTox 3.0 (Banerjee et al., 2024). The findings indicated that as the transformation pathways progressed, the LD<sub>50</sub> values of the products generally increased, except for 2,5-Cl<sub>2</sub>Fluor, indicating a general toxicity decrement alongside XPAH transformation. For instance, the LD<sub>50</sub> of 9,10-Cl<sub>2</sub>Phe was 886 mg/kg with a toxicity level of 4. Among its transformation products, only B1 (Phe) had an LD<sub>50</sub> (316 mg/kg, level 4) lower than that of 9,10-Cl<sub>2</sub>Phe, while the toxicities of other oxidation and ring-opening products were lower. However, previous studies on the aryl hydrocarbon receptor activities of XPAHs in yeast assays reported the opposite results on toxicities of 9,10-Cl<sub>2</sub>Phe and Phe: the relative equivalent potency of 9,10-Cl<sub>2</sub>Phe was found to be much higher than Phe. In the case of 2,5-Cl<sub>2</sub>Fluor, its inherently high LD<sub>50</sub> (4220 mg/kg, level 5) resulted in most of its products having higher toxicity levels compared to the parent compound. Overall, most transformation products have toxicity levels lower than their precursors. However, given the disparities between model predictions and experimental results, further toxicity experiments are needed to substantiate the changes in toxicity during the transformation process of XPAHs.





425 **Fig. 6.** (a) Prediction of environmental behaviors of XPAHs and their transformation products. (b) Respiratory  
426 toxicities (LD50) of XPAHs and their transformation products predicted by ProTox 3.0 model.

#### 427 **4. Conclusion**

428 In summary, this study elucidated the mechanisms, influencing factors, pathways, and products  
429 involved in the conversion of XPAHs on PM through comprehensive field sampling and laboratory  
430 simulations. Experimental findings revealed that the molecular structures of PAHs exerted a significant  
431 influence on the conversion process, with dehalogenation and cleavage of the parent ring structure being  
432 prominent features of XPAHs conversion. The number and position of substituents further modulated the  
433 conversion dynamics. Key environmental parameters, including humidity, temperature, and H<sub>2</sub>O<sub>2</sub>  
434 concentration, were identified as critical factors impacting conversion efficiency. The resulting  
435 conversion products and pathways were systematically hypothesized and confirmed, indicating a  
436 progressive decrease in environmental risks associated with the products as conversion advanced. This  
437 study provided novel insights into the heterogeneous conversion mechanisms of XPAHs on particulate  
438 matter, offering valuable contributions to the understanding of their environmental behavior and impact.

#### 441 **ASSOCIATED CONTENT**

##### 442 **Author contributions**

443 YY, RJ and MZ conceived the study and wrote the paper, YY, YL, GZ, SZ and XL performed the  
444 measurements and collected data. All authors contributed to the data analysis and review of the paper.

##### 445 **Competing Interests**

446 The authors declare that they have no conflict of interest.

##### 447 **Data availability**

448 All data are available from the authors upon request by contacting Rong Jin ([jinrong@ucas.ac.cn](mailto:jinrong@ucas.ac.cn)).

##### 449 **Supporting information**

450 Including detailed information on chemicals, sample testing and analysis data, screening of  
451 chemical properties and toxicity prediction information, relevant parameters and data from simulation



452 experiments, as well as chromatograms for product identification.

453 **Acknowledgement**

454 The authors acknowledge the financial support provided by the Natural Science Foundation of Zhejiang  
455 Province (Grant No. LQ22B070009), the National Natural Science Foundation of China (Grant No.  
456 22106030), "Pioneer" and "Leading Goose" R&D Program of Zhejiang (Grant No. 2023C03157) and the  
457 Research Funds of Hangzhou Institute for Advanced Study, UCAS (Grant No. 2023HIAS-Y014,  
458 2022ZZ01017).



## 459 References

- 460 Banerjee, P., Kemmler, E., Dunkel, M., Preissner, R., 2024. ProTox 3.0: a webserver for the prediction of  
 461 toxicity of chemicals. *Nucleic. Acids. Res.*, 52, 1-8. <https://doi.org/10.1093/nar/gkac303>
- 462 Cao, Q., Liu, Y., Lyu, K., Yu, Y., Li, D., Yang, L., 2020. Solar radiation zoning and daily global radiation  
 463 models for regions with only surface meteorological measurements in China. *Energy Conversion*  
 464 *and Management* 225, 113447. <https://doi.org/10.1016/j.enconman.2020.113447>
- 465 Concha, C., Manzano, C., 2023. Priority pesticides in Chile: Predicting their environmental distribution,  
 466 bioaccumulation, and transport potential. *Integr. Environ. Assess. Manag.* 19, 676-683.  
 467 <https://doi.org/10.1002/ieam.4680>
- 468 Dang, J., Shi, X., Zhang, Q., Hu, J., Chen, J., Wang, W., 2014. Mechanistic and kinetic studies on the  
 469 OH-initiated atmospheric oxidation of fluoranthene. *Sci. Total. Environ.* 490, 639-646.  
 470 <https://doi.org/10.1016/j.scitotenv.2014.04.134>
- 471 Deng, Q., Feng, J., Gao, P., Ni, H., 2023. Combined effects of vehicles and waste incineration on urban  
 472 air halogenated and parent polycyclic aromatic hydrocarbons. *Environ. Int.* 171, 107720.  
 473 <https://doi.org/10.1016/j.envint.2022.107720>
- 474 Hu, W., Liu, D., Su, S., Ren, L., Ren, H., Wei, L., Yue, S., Xie, Q., Zhang, Z., Wang, Z., Yang, N., Wu,  
 475 L., Deng, J., Qi, Y., Fu, P., 2021. Photochemical degradation of organic matter in the atmosphere.  
 476 *Adv. Sustain. Syst.* 5, 21000027. <https://doi.org/10.1002/adsu.202100027>
- 477 Jia, H., Zhao, S., Shi, Y., Zhu, K., Gao, P., Zhu, L., 2019. Mechanisms for light-driven evolution of  
 478 environmentally persistent free radicals and photolytic degradation of PAHs on Fe(III)-  
 479 montmorillonite surface. *J. Hazard. Mater.* 362, 92-98.  
 480 <https://doi.org/10.1016/j.jhazmat.2018.09.019>
- 481 Jin, R., Liu, G., Jiang, X., Liang, Y., Fiedler, H., Yang, L., Zhu, Q., Xu, Y., Gao, L., Su, G., Xiao, K.,  
 482 Zheng, M., 2017. Profiles, sources and potential exposures of parent, chlorinated and brominated  
 483 polycyclic aromatic hydrocarbons in haze associated atmosphere. *Sci. Total. Environ.* 593-594,  
 484 390-398. <https://doi.org/10.1016/j.scitotenv.2017.03.134>
- 485 Jin, R., Liu, G., Zheng, M., Jiang, X., Zhao, Y., Yang, L., Wu, X., Xu, Y., 2017. Secondary copper  
 486 smelters as sources of chlorinated and brominated polycyclic aromatic hydrocarbons. *Environ.*  
 487 *Sci. Technol.* 51, 7945-7953. <https://doi.org/10.1021/acs.est.7b02031>
- 488 Jin, R., Liu, G., Zhou, X., Zhang, Z., Lin, B., Liu, Y., Qi, Z., Zheng, M., 2023. Analysis of polycyclic  
 489 aromatic hydrocarbon derivatives in environment. *TrAC-Trend Anal.* 160, 116942.  
 490 <https://doi.org/10.1016/j.trac.2023.116942>
- 491 Jin, R., Yang, L., Zheng, M., Xu, Y., Li, C., Liu, G., 2018. Source identification and quantification of  
 492 chlorinated and brominated polycyclic aromatic hydrocarbons from cement kilns co-processing  
 493 solid wastes. *Environ. Pollut.* 242, 1346-1352. <https://doi.org/10.1016/j.envpol.2018.08.025>
- 494 Jin, R., Zheng, M., Lammel, G., Bandowe, B., Liu, G., 2020. Chlorinated and brominated polycyclic  
 495 aromatic hydrocarbons: Sources, formation mechanisms, and occurrence in the environment.  
 496 *Prog. Energ. Combust.* 76, 100803. <https://doi.org/10.1016/j.peccs.2019.100803>
- 497 Jin, R., Zheng, M., Yang, H., Yang, L., Wu, X., Xu, Y., Liu, G., 2017. Gas-particle phase partitioning  
 498 and particle size distribution of chlorinated and brominated polycyclic aromatic hydrocarbons in  
 499 haze. *Environ. Pollut.* 231, 1601-1608. <https://doi.org/10.1016/j.envpol.2017.09.066>
- 500 Kakimoto, K., Nagayoshi, H., Konishi, Y., Kajimura, K., Ohura, T., Hayakawa, K., Toriba, A., 2014.  
 501 Atmospheric chlorinated polycyclic aromatic hydrocarbons in East Asia. *Chemosphere* 111, 40-  
 502 46. <https://doi.org/10.1016/j.chemosphere.2014.03.072>



- 503 Kang, Q., Bao, S., Chen, B., 2021. Phototransformation of three polychlorinated naphthalenes on surface  
504 of atmospheric particulate matter. *J. Hazard. Mater.* 409, 124895.  
505 <https://doi.org/10.1016/j.jhazmat.2020.124895>
- 506 Kitazawa, A., Amagai, T., Ohura, T., 2006. Temporal trends and relationships of particulate chlorinated  
507 polycyclic aromatic hydrocarbons and their parent compounds in urban air. *Environ. Sci. Technol.*  
508 40, 4592-4598.
- 509 Lara, S., Villanueva, F., Martín, P., Salgado, S., Moreno, A., Sánchez-Verdú, P., 2022. Investigation of  
510 PAHs, nitrated PAHs and oxygenated PAHs in PM10 urban aerosols. A comprehensive data  
511 analysis. *Chemosphere* 294, 133745. <https://doi.org/10.1016/j.chemosphere.2022.133745>
- 512 Laskin, A., Laskin, J., Nizkorodov, S., 2015. Chemistry of atmospheric brown carbon. *Chem. Rev.* 115,  
513 4335-4382. <https://doi.org/10.1021/cr5006167>
- 514 Li, X., Abdullah, L., Sobri, S., Md Said, M., Hussain, S., Aun, T., Hu, J., 2023. Long-term air pollution  
515 characteristics and multi-scale meteorological factor variability analysis of mega-mountain cities  
516 in the chengdu-chongqing economic circle. *Water Air Soil Pollut.* 234, 328.  
517 <https://doi.org/10.1007/s11270-023-06279-8>
- 518 Liu, Q., Liggio, J., Li, K., Lee, P., Li, S., 2019. Understanding the impact of relative humidity and  
519 coexisting soluble iron on the oh-initiated heterogeneous oxidation of organophosphate flame  
520 retardants. *Environ. Sci. Technol.* 53, 6794-6803. <https://doi.org/10.1021/acs.est.9b01758>
- 521 Liu, Q., Xu, X., Wang, L., Lin, L., Wang, D., 2019. Simultaneous determination of forty-two parent and  
522 halogenated polycyclic aromatic hydrocarbons using solid-phase extraction combined with gas  
523 chromatography-mass spectrometry in drinking water. *Ecotoxicol. Environ. Saf.* 181, 241-247.  
524 <https://doi.org/10.1016/j.ecoenv.2019.06.011>
- 525 Ma, J., Chen, Z., Wu, M., Feng, J., Horii, Y., Ohura, T., Kannan, K., 2013. Airborne PM2.5/PM10-  
526 associated chlorinated polycyclic aromatic hydrocarbons and their parent compounds in a  
527 suburban area in Shanghai, China. *Environ. Sci. Technol.* 47, 7615-7623.  
528 <https://doi.org/10.1021/es400338h>
- 529 Malecha, K., Nizkorodov, S., 2016. Photodegradation of secondary organic aerosol particles as a source  
530 of small, oxygenated volatile organic compounds. *Environ. Sci. Technol.* 50, 9990-9997.  
531 <https://doi.org/10.1021/acs.est.6b02313>
- 532 Nilsson, U., Ostman, C., 1993. Chlorinated polycyclic aromatic-hydrocarbons - method of analysis and  
533 their occurrence in urban air. *Environ. Sci. Technol.* 27, 1826-1831.  
534 <https://doi.org/10.1021/es00046a010>
- 535 Nishimura, C., Horii, Y., Tanaka, S., Asante, K., Ballesteros, F., Jr., Viet, P., Itai, T., Takigami, H., Tanabe,  
536 S., Fujimori, T., 2017. Occurrence, profiles, and toxic equivalents of chlorinated and brominated  
537 polycyclic aromatic hydrocarbons in E-waste open burning soils. *Environ. Pollut.* 225, 252-260.  
538 <https://doi.org/10.1016/j.envpol.2016.10.088>
- 539 Noro, K., Omagari, R., Ito, K., Wang, Q., Sei, K., Miyake, Y., Amagai, T., 2023. Sampling, pretreatment,  
540 instrumental analysis, and observed concentrations of polycyclic aromatic hydrocarbons,  
541 polychlorinated naphthalenes, and halogenated polycyclic aromatic hydrocarbons: A review.  
542 *TrAC-Trend Anal. Chem.* 169, 117384. <https://doi.org/10.1016/j.trac.2023.117384>
- 543 Ohura, T., Amagai, T., Makino, M., 2008. Behavior and prediction of photochemical degradation of  
544 chlorinated polycyclic aromatic hydrocarbons in cyclohexane. *Chemosphere* 70, 2110-2117.  
545 <https://doi.org/10.1016/j.chemosphere.2007.08.064>
- 546 Ohura, T., Horii, Y., Kojima, M., Kamiya, Y., 2013. Diurnal variability of chlorinated polycyclic  
547 aromatic hydrocarbons in urban air, Japan. *Atmos. Environ.* 81, 84-91.





- 548 <https://doi.org/10.1016/j.atmosenv.2013.08.044>
- 549 Ohura, T., Morita, M., Makino, M., Amagai, T., Shimoi, K., 2007. Aryl hydrocarbon receptor-mediated  
550 effects of chlorinated polycyclic aromatic hydrocarbons. *Chem. Res. Toxicol.* 20, 1237–1241.
- 551 Ohura, T., Sakakibara, H., Watanabe, I., Shim, W., Manage, P., Guruge, K., 2015. Spatial and vertical  
552 distributions of sedimentary halogenated polycyclic aromatic hydrocarbons in moderately  
553 polluted areas of Asia. *Environ. Pollut.* 196, 331-340.  
554 <https://doi.org/10.1016/j.envpol.2014.10.028>
- 555 Ohura, T., Savada, K., Amagai, T., Shinomiya, M., 2009. Discovery of novel halogenated polycyclic  
556 aromatic hydrocarbons in urban particulate matters: occurrence, photostability, and ahr activity.  
557 *Environ. Sci. Technol.* 43, 2269–2275.
- 558 Sei, K., Wang, Q., Tokumura, M., Miyake, Y., Amagai, T., 2021. Accurate and ultrasensitive  
559 determination of 72 parent and halogenated polycyclic aromatic hydrocarbons in a variety of  
560 environmental samples via gas chromatography-triple quadrupole mass spectrometry.  
561 *Chemosphere* 271, 129535. <https://doi.org/10.1016/j.chemosphere.2021.129535>
- 562 Shiraishi, H., Pilkington, N., Otsuki, A., Fuwa, K., 1985. Occurrence of chlorinated polynuclear  
563 aromatic hydrocarbons in tap water. *Environ. Sci. Technol.* 19, 585-590.  
564 <https://doi.org/10.1021/es00137a001>
- 565 Shiraiwa, M., Ammann, M., Koop, T., Pöschl, U., 2011. Gas uptake and chemical aging of semisolid  
566 organic aerosol particles. *Proc. Natl. Acad. Sci. USA* 108, 11003-11008.  
567 <https://doi.org/10.1073/pnas.1103045108>
- 568 Sun, J., Zeng, H., Ni, H., 2013. Halogenated polycyclic aromatic hydrocarbons in the environment.  
569 *Chemosphere* 90, 1751-1759. <https://doi.org/10.1016/j.chemosphere.2012.10.094>
- 570 Takikawa, T., Wang, Q., Omagari, R., Noro, K., Miyake, Y., Amagai, T., 2023. Development of an  
571 analytical method for indoor polycyclic aromatic hydrocarbons and their halogenated derivatives  
572 by using thermal separation probe coupled to gas chromatography-tandem mass spectrometry.  
573 *Sci. Total. Environ.* 903, 166931. <https://doi.org/10.1016/j.scitotenv.2023.166931>
- 574 Vuong, Q., Thang, P., Nguyen, T., Ohura, T., Choi, S., 2020. Seasonal variation and gas/particle  
575 partitioning of atmospheric halogenated polycyclic aromatic hydrocarbons and the effects of  
576 meteorological conditions in Ulsan, South Korea. *Environ. Pollut.* 263, 114592.  
577 <https://doi.org/10.1016/j.envpol.2020.114592>
- 578 Wang, T., Liu, Y., Deng, Y., Cheng, H., Yang, Y., Feng, Y., Zhang, L., Fu, H., Chen, J., 2020.  
579 Photochemical oxidation of water-soluble organic carbon (WSOC) on mineral dust and enhanced  
580 organic ammonium formation. *Environ. Sci. Technol.* 54, 15631-15642.  
581 <https://doi.org/10.1021/acs.est.0c04616>
- 582 Wang, Y., Su, P., Ge, X., Ren, H., Ma, S., Shen, G., Chen, Q., Yu, Y., An, T., 2022. Identification of  
583 specific halogenated polycyclic aromatic hydrocarbons in surface soils of petrochemical, flame  
584 retardant, and electronic waste dismantling industrial parks. *J. Hazard. Mater.* 436, 129160.  
585 <https://doi.org/10.1016/j.jhazmat.2022.129160>
- 586 Xia, Z., Idowu, I., Marvin, C., Thomas, P., Johnson, W., Francisco, O., Stetefeld, J., Crimmins, B., Fry,  
587 M., Tomy, G., 2019. Identification of halogenated polycyclic aromatic hydrocarbons in biological  
588 samples from Alberta Oil-Sands Region. *Chemosphere* 215, 206-213.  
589 <https://doi.org/10.1016/j.chemosphere.2018.10.050>
- 590 Xie, J., Tao, L., Wu, Q., Lei, S., Lin, T., 2021. Environmental profile, distributions and potential sources  
591 of halogenated polycyclic aromatic hydrocarbons. *J. Hazard. Mater.* 419, 126164.  
592 <https://doi.org/10.1016/j.jhazmat.2021.126164>





- 593 Yang, L., Shen, J., Zheng, M., Yang, Q., Li, D., Liu, G., 2022. Occurrence of chlorinated and brominated  
594 polycyclic aromatic hydrocarbons from electric arc furnace for steelmaking. *Environ. Pollut.* 294,  
595 118663. <https://doi.org/10.1016/j.envpol.2021.118663>
- 596 Yang, Y., Liu, G., Zheng, M., Liu, S., Yang, Q., Liu, X., Wang, M., Yang, L., 2022. Discovery of  
597 significant atmospheric emission of halogenated polycyclic aromatic hydrocarbons from  
598 secondary zinc smelting. *Ecotoxicol. Environ. Saf.* 238, 113594.  
599 <https://doi.org/10.1016/j.ecoenv.2022.113594>
- 600 Zhang, L., Yan, W., Kohtani, S., Fukuyoshi, S., Hu, M., Nagao, S., Tang, N., 2024. Promotive effects of  
601 marine-derived dimethyl sulfoxide on the photodegradation of phenanthrene in the atmosphere.  
602 *Sci. Total. Environ.* 926, 171938. <https://doi.org/10.1016/j.scitotenv.2024.171938>
- 603 Zhang, L., Li, P., Gong, Z., Oni, A., 2006. Photochemical behavior of benzo[a]pyrene on soil surfaces  
604 under UV light irradiation. *J. Environ. Sci. (China)* 18, 1226-1232.  
605 [https://doi.org/10.1016/s1001-0742\(06\)60067-3](https://doi.org/10.1016/s1001-0742(06)60067-3)
- 606 Zhang, Q., Wang, Y., Gao, M., Li, Y., Zhao, L., Yao, Y., Chen, H., Wang, L., Sun, H., 2023.  
607 Organophosphite antioxidants and novel organophosphate esters in dust from china: large-scale  
608 distribution and heterogeneous phototransformation. *Environ. Sci. Technol.* 57, 4187-4198.  
609 <https://doi.org/10.1021/acs.est.2c08239>
- 610 Zhao, S., Jia, H., Nulaji, G., Gao, H., Wang, F., Wang, C., 2017. Photolysis of polycyclic aromatic  
611 hydrocarbons (PAHs) on Fe<sup>(3+)</sup>-montmorillonite surface under visible light: Degradation kinetics,  
612 mechanism, and toxicity assessments. *Chemosphere* 184, 1346-1354.  
613 <https://doi.org/10.1016/j.chemosphere.2017.06.106>
- 614 Zhu, J., Sheng, M., Shang, J., Kuang, Y., Shi, X., Qiu, X., 2022. Photocatalytic role of atmospheric soot  
615 particles under visible-light irradiation: reactive oxygen species generation, self-oxidation  
616 process, and induced higher oxidative potential and cytotoxicity. *Environ. Sci. Technol.* 56,  
617 7668-7678. <https://doi.org/10.1021/acs.est.2c00420>